

Planetary Scale Selection of the Madden–Julian Oscillation*

TIM LI AND CHUNHUA ZHOU

Department of Meteorology, University of Hawaii at Manoa, Honolulu, Hawaii

(Manuscript received 1 October 2008, in final form 24 December 2008)

ABSTRACT

Numerical experiments with a 2.5-layer and a 2-level model are conducted to examine the mechanism for the planetary scale selection of the Madden–Julian oscillation (MJO). The strategy here is to examine the evolution of an initial perturbation that has a form of the equatorial Kelvin wave at zonal wavenumbers of 1 to 15. In the presence of a frictional boundary layer, the most unstable mode prefers a short wavelength under a linear heating; but with a nonlinear heating, the zonal wavenumber 1 grows fastest. This differs significantly from a model without the boundary layer, in which neither linear nor nonlinear heating leads to the long wave selection. Thus, the numerical simulations point out the crucial importance of the combined effect of the nonlinear heating and the frictional boundary layer in the MJO planetary scale selection.

The cause of this scale selection under the nonlinear heating is attributed to the distinctive phase speeds between the dry Kelvin wave and the wet Kelvin–Rossby wave couplet. The faster dry Kelvin wave triggered by a convective branch may catch up and suppress another convective branch, which travels ahead of it at the phase speed of the wet Kelvin–Rossby wave couplet if the distance between the two neighboring convective branches is smaller than a critical distance (about 16 000 km). The interference between the dry Kelvin wave and the wet Kelvin–Rossby wave couplet eventually dissipates and “filters out” shorter wavelength perturbations, leading to a longwave selection. The boundary layer plays an important role in destabilizing the MJO through frictional moisture convergences and in retaining the in-phase zonal wind–pressure structure.

1. Introduction

An outstanding question about the Madden–Julian Oscillation (MJO; Madden and Julian 1971, 1972) is why the oscillation prefers a planetary zonal scale. There have been a number of theoretical studies aimed at addressing this scale selection issue. Chang (1977) proposed that the MJO can be represented by convectively driven equatorial Kelvin waves. However, the wave–conditional instability of second kind (CISK) mechanism prefers the most unstable growth at a shorter zonal wavelength. Lau and Peng (1987), Chang and Lim (1988), and Lim et al. (1990) demonstrated in numerical models that the Kelvin wave with a zonal wavenumber-1

structure is selectively amplified when a positive-only condensational heating is applied. Using a linear 2.5-layer model that consists of a two-level free atmosphere and a well-mixed planetary boundary layer (PBL), Wang (1988) showed that the instability of the MJO may arise from the boundary layer friction-induced moisture convergence. A preferred planetary zonal wavelength may be derived when a low-frequency (40–50 day) period is specified. This did not completely solve the scale selection problem because the temporal and spatial scales of unstable modes are related. As shown in this paper, the 2.5-layer model does not favor a planetary zonal scale under a linear heating. Wang and Xue (1992) further studied the instability property in a two-level model with a nonlinear positive-only conditional heating. In the absence of the atmospheric boundary layer, a zonal wavenumber-1 structure emerges in a weak growth regime. For the most unstable mode, however, there is no planetary scale selection. Goswami and Rao (1994) presented a mechanism for selective excitation of the equatorial Kelvin wave at the period of 30–50 days when a time lag between the convection and the heating is assumed. Xie (1994) noted that the MJO zonal length

* School of Ocean and Earth Science and Technology Contribution Number 7674; International Pacific Research Center Contribution Number 606.

Corresponding author address: Dr. Tim Li, Department of Meteorology, University of Hawaii at Manoa, 2525 Correa Rd., Honolulu, HI 96822.
E-mail: timli@hawaii.edu

scale is sensitive to the model horizontal resolution. Observational, theoretical, and modeling studies revealed the multiscale interaction nature of the MJO (e.g., Nakazawa 1988; Grabowski 2001; Moncrieff 2004; Khouider and Majda 2006, 2007; Biello et al. 2007). Based on the scale interaction model of Majda and Biello (2004) and Biello and Majda (2005), Majda and Stechmann (2009) examined the role of upscale and downscale momentum transport of convectively coupled synoptic waves in the intraseasonal oscillation and argued that the second baroclinic heating is key to longwave instabilities in the tropical atmosphere.

Although many numerical studies have pointed out the importance of the nonlinear positive-only heating in the MJO scale selection, it is not clear how the nonlinear heating leads to the planetary scale selection. This motivates us to address this issue in the current study. Another key process related to MJO is the effect of the planetary boundary layer. Several observational and theoretical studies (e.g., Hendon and Salby 1994; Wang and Li 1994; Waliser et al. 1999; Maloney 2002) illustrated a remarkable phase difference between the MJO convection and the boundary layer convergence. Is the inclusion of a frictional boundary layer dynamically essential for causing the planetary spatial scale?

In this study we revisit this outstanding MJO scale selection problem with a special focus on the role of the nonlinear heating and the atmospheric boundary layer. The rest of the paper is organized as follows: The numerical models and experiment design are introduced in section 2. In section 3 we present results from a 2.5-layer model with an emphasis on the effect of the nonlinear heating. In section 4 we compare the 2.5-layer model simulation with that from a two-level model to reveal the role of the PBL. Sensitivity experiments are further conducted and analyzed in section 5. Finally, a summary and discussions are provided in section 6.

2. Numerical models and strategy

Given the observed vertical structure of the MJO (Hendon and Salby 1994), the simplest dynamic framework consists of the first baroclinic mode free atmosphere and a well-mixed boundary layer (Wang 1988; Li and Wang 1994a). Thus the numerical model used here is the finite difference form of the 2.5-layer atmosphere model of Li and Wang (1994a). The governing equations may be written as

$$\begin{aligned} \frac{\partial \mathbf{V}}{\partial t} &= -f\mathbf{k} \times \mathbf{V} - \nabla\phi, \\ \frac{\partial \phi}{\partial t} + C_0^2(1 - \delta I)\nabla \cdot \mathbf{V} &= C_0^2(\delta B - 1)\nabla \cdot \mathbf{V}_B, \quad \text{and} \\ E\mathbf{V}_B + f\mathbf{k} \times \mathbf{V}_B &= -\nabla\phi, \end{aligned} \quad (1)$$

where \mathbf{V} and \mathbf{V}_B denote the lower tropospheric and boundary layer winds; ϕ denotes the lower tropospheric geopotential height; f , C_0 , and E are the Coriolis parameter, first-baroclinic mode gravity wave speed, and Ekman frictional coefficient; and I and B are the convective heating coefficients contributed by the wave convergence and boundary layer frictional convergence, respectively (Wang 1988).

The condensational heating rate in the middle troposphere is proportional to the vertically integrated moisture convergence:

$$Q'_m = \frac{\delta b L_c}{\Delta p} [-\omega'_m(\bar{q}_2 - \bar{q}_1) - \omega'_e(\bar{q}_e - \bar{q}_2)], \quad (2)$$

where δ is an SST-dependent conditional heating coefficient [see Eq. (4.3) in Wang and Li 1993]. This SST-dependent positive-only conditional heating is approximately equivalent to the convective instability criterion for the tropical low-frequency motion because on monthly or longer time scales the surface moisture and air temperature are in general in equilibrium with SST. In the current study, a constant SST of 29°C is specified, and the heating is separated into a nonlinear and linear heating. For the nonlinear heating (i.e., conditional positive-only heating), δ is unity at the vertically integrated moisture convergence region and zero at the vertically integrated moisture divergence region. Because the model does not contain nonlinear advection terms, the positive-only heating is the only term that represents a nonlinear effect in the system. [For a discussion of the reasons for dropping the nonlinear advection terms, readers are referred to Wang and Li (1993) and Li and Wang (1994b).] For the linear heating, δ is always unity, no matter whether the vertically integrated moisture divergence is positive or negative; Δp (=400 hPa) is the mean depth between the two free atmosphere layers; \bar{q}_1 , \bar{q}_2 , and \bar{q}_e denote the mean specific humidity field in the upper troposphere, lower troposphere, and PBL respectively; the background humidity field is the function of the surface humidity and decays exponentially with height (Wang 1988); ω'_m and ω'_e are the vertical velocities in the middle troposphere and at the top of the PBL, respectively; $b = 0.9$ is a fraction factor that measures how much the convergent moisture is condensed out as precipitation; and L_c is the latent heat of condensation per unit mass.

The model covers a domain of (40°S–40°N, 0°–360°E) with a horizontal resolution of 5° longitude \times 2° latitude. A central difference scheme with Robert filtering is used for time integration and each time step is 10 min. A Newtonian damping or Rayleigh friction term (with a

weak damping coefficient of $2 \times 10^{-6} \text{ s}^{-1}$) and a horizontal diffusion term are included in the free atmospheric momentum and thermodynamic equation. The initial perturbation is specified in the form of an equatorial Kelvin wave, which has an in-phase relationship between the zonal wind and geopotential height fields and a vanished meridional wind component, with maximum amplitude of the zonal wind and geopotential height fields right on the equator (Matsuno 1966). Observations (e.g., Hendon and Salby 1994) indicate that the horizontal structure of the MJO resembles a convectively coupled Kelvin–Rossby wave couplet. Although free Kelvin and Rossby waves may propagate in an opposite direction, it is the convective heating that holds them together. The numerical simulations with the 2.5-layer model framework (e.g., Wang and Li 1994; Li and Wang 1994a) exhibit a similar Kelvin–Rossby wave couplet structure. Even though a Kelvin wave is introduced initially, the Kelvin–Rossby wave couplet pattern is quickly set up in the model because of the convective heating. The phase speed of this wet Kelvin–Rossby wave couplet is somewhat slower than a pure wet Kelvin wave because of its dispersive character (Wang and Li 1994).

It is worth mentioning that the current study aims to understand the MJO planetary scale selection—that is, how the growth rate of the unstable equatorial mode depends on the mode’s wavelength. Our purpose is not to simulate as realistic an MJO as possible; rather we study this fundamental scale selection problem in the simplest model possible. This is why we specify a constant SST in the model with no basic-state flows. The roles of realistic SST and surface moisture distributions and 3D mean flows on MJO phase propagation and evolution have been investigated in a similar 2.5-layer framework (in which MJO convection travels slowly over the Indian Ocean and western Pacific warm pool, dissipates in the eastern Pacific cold tongue, and reinitiates in the western Indian Ocean) by Li and Wang (1994a) and Wang and Xie (1997).

To reveal the role of the PBL, a two-level free atmospheric model without a boundary layer is constructed for comparison. The governing equation for the two-level model is essentially same as (1) except that we set $\mathbf{V}_B = 0$. The nonlinear condensational heating rate is expressed as

$$Q'_m = -\frac{\delta b L_\varepsilon}{\Delta p} \omega'_m (\bar{q}_2 - \bar{q}_1). \quad (3)$$

To illustrate how the zonal scale of the most unstable mode is selected, our strategy is to examine the time evolution of the initial Kelvin wave perturbation that

has different zonal wavelengths ranging from zonal wavenumbers 1 to 15 under linear or nonlinear heating and with or without the atmospheric PBL. Through the detailed diagnosis of the model outputs, we illustrate the fundamental role of the nonlinear heating and the boundary layer dynamics in determining the MJO scale selection.

3. Role of nonlinear heating

In this section we examine the role of nonlinear heating by analyzing two sets of numerical simulations from the 2.5-layer model. In the first set of experiments, a linear heating ($\delta = 1$) is specified. In the second set, a nonlinear, positive-only heating is specified. For each set of experiments, 15 runs are conducted, each of which has the same initial Kelvin wave structure but a different zonal wavenumber of 1, 2, . . . , 15, respectively. Each initial perturbation has the same amplitude and the same first baroclinic mode vertical structure.

a. Simulations with the linear heating

As predicted from a linear eigenvalue analysis, the numerical simulations from the first set of experiments show the exponential growth of the MJO perturbation as it propagates eastward along the equator. For the linear heating case, the model is integrated for 5 days. Because different wave components do not interfere with each other in a linear system, the perturbation keeps its initial wavenumber. Because the evolution and propagation of the perturbations bear similar features for all wavenumbers, only the model simulation from the initial wavenumber-5 perturbation case is shown in Fig. 1. Figure 1 shows the time evolution of the lower tropospheric zonal wind along the equator. The perturbation moves eastward and grows while keeping the initial wavenumber-5 structure. There is no generation of the planetary zonal scale perturbation.

To calculate the growth rate for each wavenumber, a Fourier decomposition is applied to the model zonal wind field. Figure 2 illustrates the evolution of the Fourier coefficients for zonal wavenumbers 1, 5, and 8. Note that the perturbation always retains its initial wavenumber under the linear heating. This situation is changed when the nonlinear heating is applied.

Although all initial perturbations grow under the linear heating, the growth rates at different zonal wavenumbers are different. The growth rate at each wavenumber is calculated based on the time series of the Fourier coefficient of the corresponding zonal wavenumber. Figure 3 shows the dependence of the growth rate on the wavenumber. Note that the maximum growth rate appears at wavenumber 6. This indicates that the

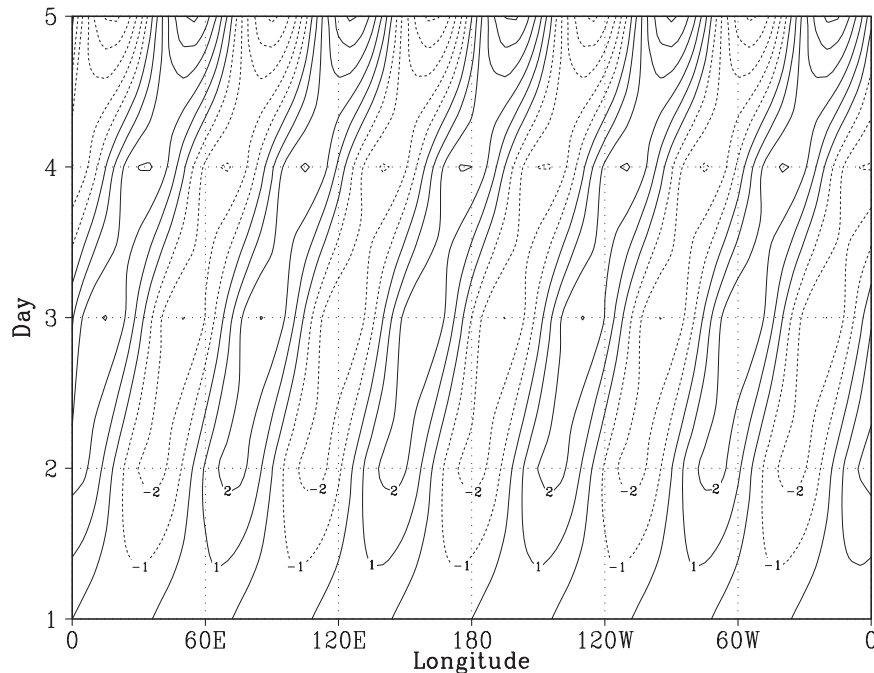


FIG. 1. Time-longitude cross section of the equatorial zonal winds from the 2.5-layer model under linear heating. An initial wavenumber-5 perturbation is specified. The contour interval is 1 m s^{-1} . The solid and dashed contour lines denote the westerly and easterly flows, respectively.

most unstable mode does not appear in the planetary zonal scale under the linear heating.

b. Simulations with the nonlinear heating

For the nonlinear, positive-only heating experiments, 15 runs with initial wavenumbers from 1 to 15 have been carried out, and for each run the model is integrated for 30 days. Figure 4 shows the simulated zonal wind field at the equator for the initial wavenumber-5 case. During the first 10 days, the perturbation retains the initial wavenumber-5 structure while propagating eastward along the equator. After this adjustment period, the amplitude of the wavenumber-5 perturbation decays and a wavenumber-1 perturbation starts to develop. By day 20, the equatorial zonal wind field is dominated by the planetary zonal scale.

The experiments with other initial wavenumbers show a similar result: no matter what initial zonal wavenumbers are given, the nonlinear heating leads to a planetary zonal scale selection at the final stage. The horizontal structure of the most unstable mode has a Kelvin-Rossby wave couplet pattern (also see Wang and Li 1994; Li and Wang 1994a), similar to the observed (e.g., Hendon and Salby 1994). The propagation speed of the couplet is slightly faster than the observed. The time to circulate around the globe is around 30–50 days, indicating the intraseasonal periodicity of the mode.

An additional experiment is carried out in which all the 15 wavenumbers with equal strength are input initially under the nonlinear heating. The evolution of the model zonal wind (Fig. 5) shows a faster-growing wavenumber-1 component compared to that in Fig. 4. For example, at day 30, the amplitude of the zonal wind is about 6 times greater. This experiment again demonstrates that when initially given wavenumbers 1–15 of equal strength, the model favors the most unstable growth of the planetary zonal scale.

To clearly illustrate how the amplitude of each wavenumber evolves with time, we plotted the time evolution of the first 10 Fourier coefficients of the equatorial zonal wind field (Fig. 6). As expected, wavenumber 1 grows fastest. The growth rate decreases with increasing zonal wavenumber. Compared to the previous linear heating cases, the second set of experiments demonstrates the role of the nonlinear heating in the planetary zonal scale selection.

To show more clearly how the nonlinear heating contributes to the longwave selection, we conducted a combined linear and nonlinear heating experiment. Initially a wavenumber-5 perturbation is introduced. A linear heating is specified for the first 4 days and then the heating is switched to nonlinear. This experiment is designed to allow the initial perturbation to grow into a finite amplitude so that one may examine clearly how

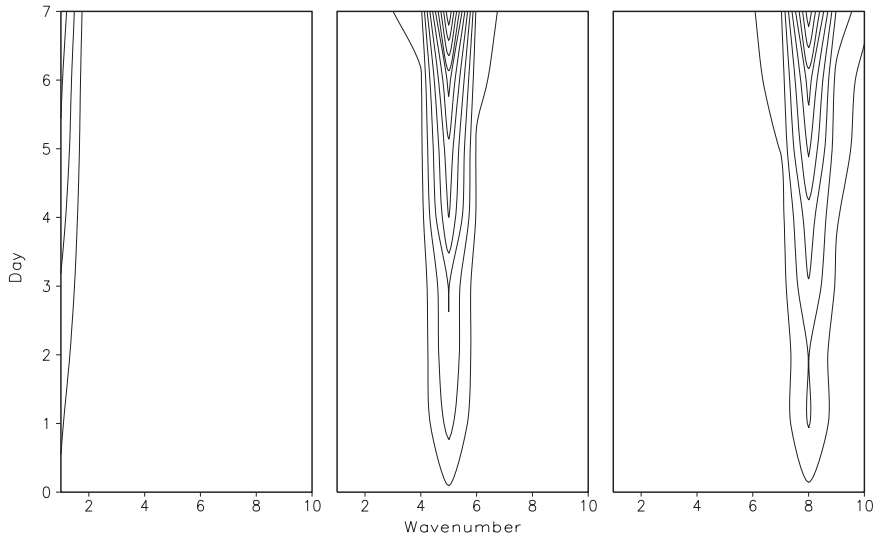


FIG. 2. Time evolution of Fourier coefficients of the equatorial zonal wind field from the 2.5-layer model for the initial wavenumber (left)-1, (middle)-5, and (right)-8 perturbations. A linear heating is specified. The contour interval is 0.5 m s^{-1} .

the finite-amplitude short-wavelength perturbation is dissipated and how a planetary scale disturbance emerges and grows. As seen from the time–longitude section of the zonal wind (Fig. 7), the initial wavenumber-5 perturbation grows under the linear heating during the first 4 days. After that, the perturbation undergoes an adjustment period as the nonlinear heating is taking into effect. A wavenumber-1 perturbation grows rapidly at the latter stage (Fig. 7).

Figure 8 illustrates the time evolution of the first and fifth Fourier coefficients of the zonal wind field at the equator. Initially the wavenumber-5 amplitude grows fast in the first 4 days. During a transition period (days 4

to 20), the wavenumber-5 amplitude decreases gradually, while the wavenumber-1 amplitude increases exponentially. After this period, wavenumber 1 dominates the zonal wind field.

To better illustrate its zonal pattern, a normalized zonal wind field is plotted along the equator at days 5, 10, 20, and 40 (Fig. 9). At day 5, the zonal wind exhibits a clear wavenumber-5 structure. This wavenumber-5 structure is slightly modified at day 10. By day 20 the zonal wind pattern is greatly deformed, with a maximum peak appearing around 120°E . This maximum

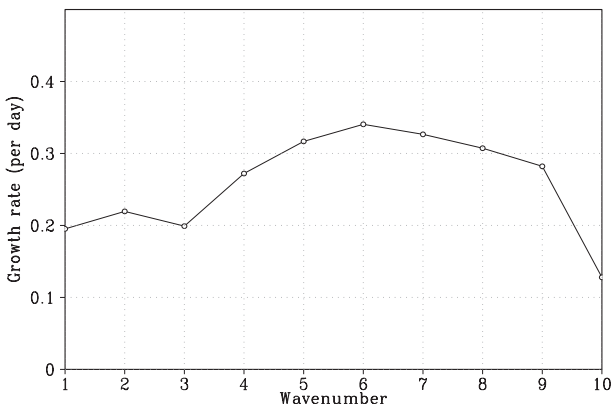


FIG. 3. Growth rate as a function of wavenumber derived from the 2.5-layer model simulations under linear heating. The horizontal axis is the initial wavenumber and the vertical axis is the growth rate (per day).

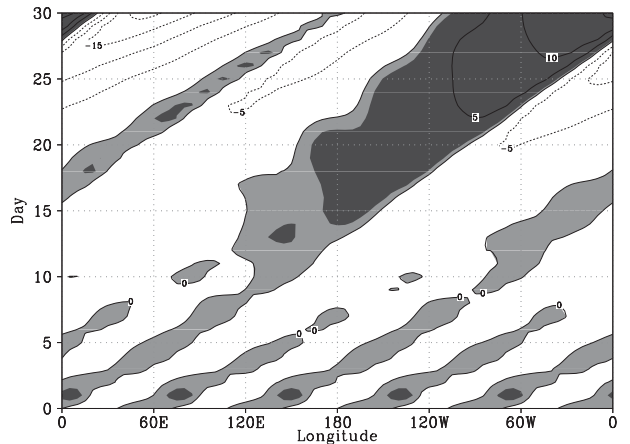


FIG. 4. Time–longitude cross section of the equatorial zonal wind in the lower troposphere from the 2.5-layer model under nonlinear heating. An initial wavenumber-5 perturbation is introduced. The contour interval is 5 m s^{-1} and the shading corresponds to the westerly wind.

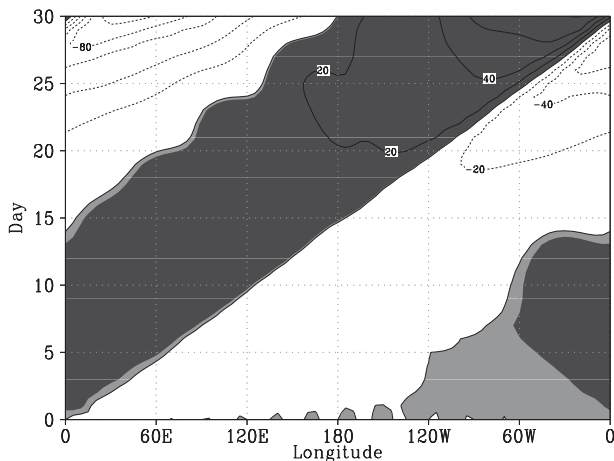


FIG. 5. As in Fig. 4, but a perturbation with combined wavenumbers 1, 2, 3, . . . , 15 is specified initially and the contour interval is 20 m s⁻¹.

peak of the zonal wind continues to grow at a rate faster than other peaks, while moving eastward. At day 40, only one maximum peak can be detected. This idealized numerical experiment clearly demonstrates a fascinating longwave selection process by the nonlinear heating.

How does the nonlinear heating cause the planetary scale selection? Figure 10 is a schematic diagram illus-

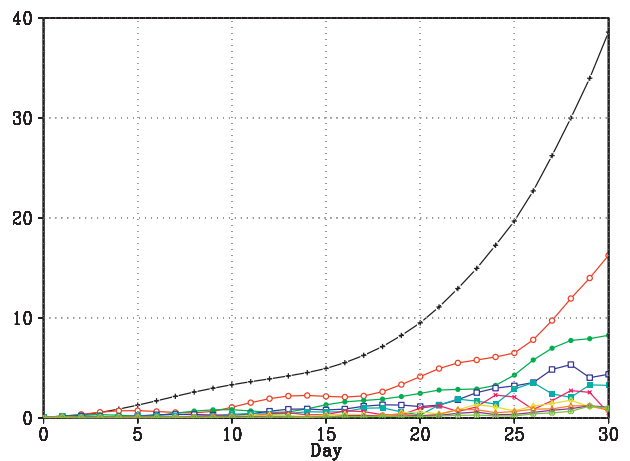


FIG. 6. Time evolution of the Fourier coefficients (m s⁻¹) for wavenumbers 1 through 10 in the 2.5-layer model under nonlinear heating. The initial condition is the same as in Fig. 5. The black line with crosses, red line with open circles, green line with closed circles, and blue line with open squares indicate wavenumbers 1, 2, 3, and 4, respectively; the other lines indicate wavenumbers 5–10.

trating how the scale selection process happens in the model. It is primarily attributed to the distinctive phase speeds between the dry Kelvin wave and the moist Kelvin–Rossby wave couplet under nonlinear heating. According to Gill (1980), convective heating at the equator may excite eastward-traveling Kelvin waves to

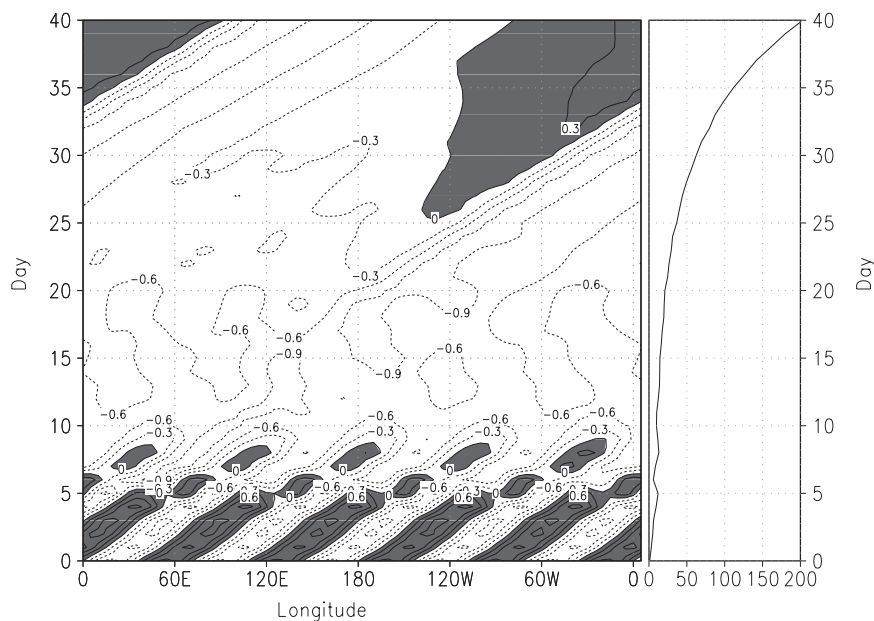


FIG. 7. (left) Time–longitude cross section of the normalized lower tropospheric zonal wind at the equator and (right) the time evolution of magnitude of the equatorial zonal wind (m s⁻¹) from the 2.5-layer model under the nonlinear heating. The initial wavenumber-5 perturbation is specified. The model is integrated for 4 days under the linear heating and then the nonlinear heating is switched on afterward. The contour interval is 0.3 and positive values are shaded.

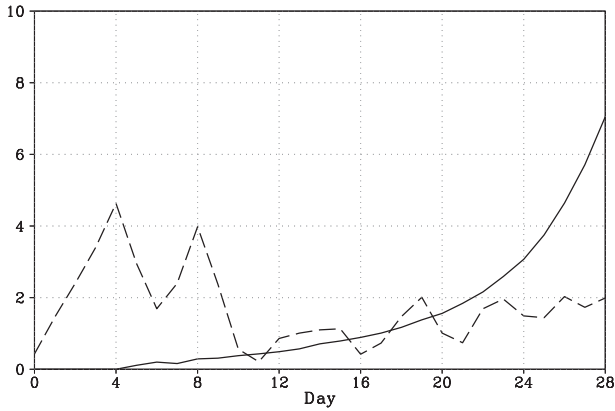


FIG. 8. Time evolution of the Fourier coefficients (m s^{-1}) of wavenumbers 1 (solid line) and 5 (dashed line) for the equatorial zonal wind from the same experiment as in Fig. 7. The zonal axis represents the model integration time from day 0 to day 28 and the vertical axis corresponds to the amplitude of the Fourier coefficients.

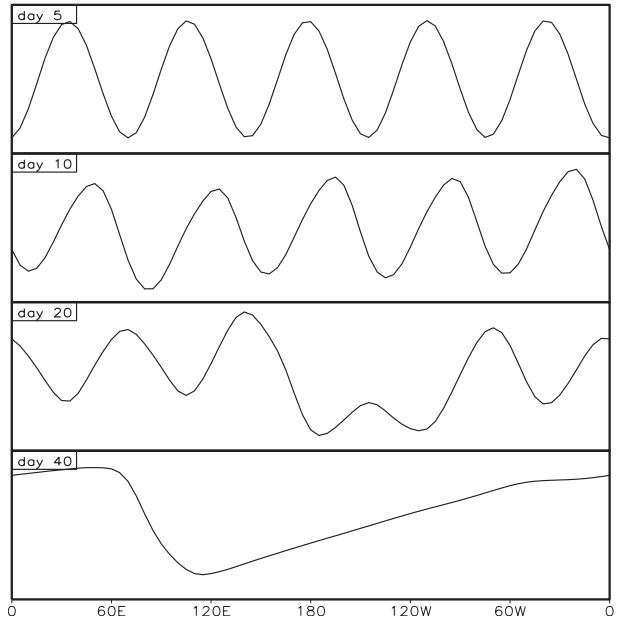


FIG. 9. Zonal pattern of the normalized lower tropospheric zonal wind at the equator at days 5, 10, 20, and 40 from the same experiment as in Fig. 7.

the east. In the presence of linear heating (i.e., $\delta \equiv 1$), the phase speed of the equatorial Kelvin waves, which is proportional to $\sqrt{1 - \delta I}$ (Wang 1988), remains the same for both the dry (suppressed convective) and wet (enhanced convective) regions. As a result, the dry and moist Kelvin waves propagate at the same speed so the dry and wet regions do not interfere with each other, no matter what the initial zonal wavenumber is. In the presence of the nonlinear, positive-only heating, the phase speeds of the dry Kelvin wave and the moist Kelvin–Rossby wave couplet are different because δ takes different values in the dry and wet regions. The phase speed of the dry Kelvin waves associated with descending motion (where $\delta = 0$) is much larger than that of the wet Kelvin–Rossby wave couplet associated

with ascending motion (or low-level convergence where $\delta = 1$) (Wang and Li 1994). Therefore, dry Kelvin waves, once excited by one convective branch, may catch up and suppress another convective branch to its east, as long as the zonal distance between the two neighboring convective branches is less than a critical distance.

This critical distance measures how far a dry Kelvin wave may propagate away from a forcing region under realistic atmospheric dissipation or friction. According to Gill (1982), the maximum impact distance for the

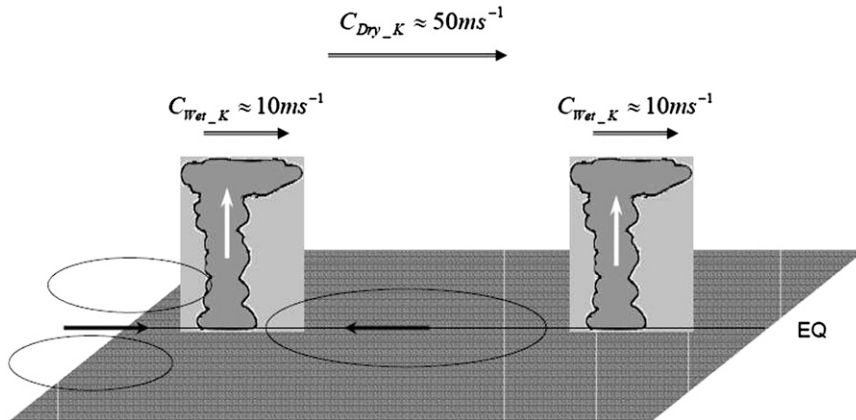


FIG. 10. Schematic diagram illustrating the role of the nonlinear heating in the MJO planetary scale selection.

Kelvin waves depends on the phase speed of the dry Kelvin wave (50 m s^{-1}) divided by a Rayleigh friction or Newtonian damping coefficient. With a realistic dissipation coefficient, Gill showed a critical distance of about 160° longitude. This implies that for perturbations with a wavelength shorter than the critical distance, the fast dry Kelvin wave may interfere and suppress the wet Kelvin–Rossby wave couplet convective branch ahead of it. Through this special scale selection process, short-wave perturbations are dissipated or cut off, whereas the planetary scale perturbations survive and grow.

In reality, a maximum convective branch may be naturally selected because of inhomogeneity in the background circulation, moisture, and land–ocean thermal distributions. With environmental factors and convective branches being equally distributed in the model, which convective branch is finally selected for the maximum growth? A diagnosis of the model simulations reveals that in all cases the initial leftmost convective branch develops fastest and becomes the dominant one at the final stage (e.g., see Fig. 4). This is because the model integration is always from the left to the right of the domain, and thus the leftmost convective branch experiences the least damping impact from the eastward-propagating dry Kelvin waves. For an initial disturbance with a zonal wavenumber greater than 2, at the final stage wavenumber 1 always dominates. For an initial wavenumber-1 or -2 perturbation, because the longitudinal distance between two neighboring convective branches is greater than the critical distance, the dry Kelvin wave and the wet Kelvin–Rossby wave couplet do not interfere with each other. In these two simulations, the initial perturbation retains its original zonal structure.

The numerical model simulations point out the importance of the nonlinear heating in the MJO planetary scale selection. Through the distinctive phase speed difference between the dry Kelvin wave and the wet Kelvin–Rossby wave couplet, the positive-only heating leads to the suppression of short waves while retaining and amplifying the planetary scale. The evidence for fast dry Kelvin waves and slower wet Kelvin–Rossby wave couplet may be discerned from the contrast of the zonal propagation speed of the rain rate field and the frontier of the zonal wind and geopotential height fields to the east of heating region (see Fig. 6 of Wang and Li 1994). Note that in the 2.5-layer model a boundary layer is included. Does a two-level model without the atmospheric PBL exhibit the same scale selection characteristic under the nonlinear heating? If no, what is the role of the boundary layer in the planetary scale selection? In the next section we further address these questions.

4. Role of the atmospheric PBL

In this section we examine the possible role of the boundary layer in the scale selection. Our strategy is to compare the 2.5-layer model simulations with those from a two-level model that excludes the effect of the frictional boundary layer. The same Kelvin wave perturbations with zonal wavenumbers from one to fifteen are introduced initially.

The two-level model solution under the linear heating is essentially the same as the free-wave solution of Matsuno (1966) except for the modulation of atmospheric stratification (or internal gravity wave speed) by diabatic heating. The amplitude of the initial perturbation decreases slightly with time because of a weak dissipation applied in the model.

The simulation of the two-level model under the nonlinear heating is shown in Fig. 11. The left side illustrates the longitude–time cross section of the equatorial zonal wind for the initial wavenumber-1 case, and the right side shows the initial wavenumber-4 case. In both the cases the zonal wind (and the geopotential height) field propagates westward at the equator after initial eastward propagation (Fig. 11). The examination of other wavenumber cases reveals the essentially same feature. The amplitude of the perturbation decreases slightly with time due to the lack of the PBL moisture convergence. Most interestingly, the initial wavenumber-4 perturbation remains the same zonal structure, and there is no planetary scale selection.

Why does the boundary layer make such a significant difference under the nonlinear heating and what causes the perturbation to move westward at the final stage? To address the questions, we examine the wind and pressure (i.e., geopotential height) tendencies associated with an initial baroclinic equatorial Kelvin wave. Figure 12 is a schematic diagram illustrating how the tendencies differ under (left) linear and (right) nonlinear heating. For simplicity, a 2D (x – z) plane and a constant heating coefficient, $I = 0.9$, are assumed here. The blue shading area in Fig. 12 represents low pressure and the red shading area represents high pressure. For the equatorial Kelvin wave, easterlies (westerlies) are in phase with low (high) pressures. According to the hydrostatic balance ($\partial\phi/\partial p = -RT/p$), the air column is warmer (colder) over the low-level low- (high) pressure and upper-level high- (low) pressure regions.

Under a realistic parameter (stable stratification) regime, the effect of adiabatic cooling dominates the effect of diabatic heating in the midtropospheric temperature equation. The adiabatic cooling (warming) associated with upward (downward) motion to the east of the low-level westerly (easterly) causes a positive (negative)

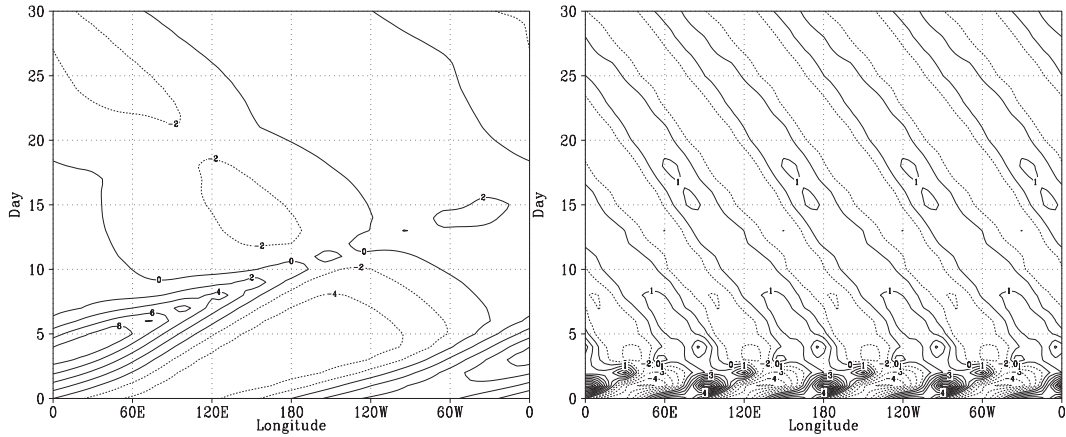


FIG. 11. Time-longitude cross section of the lower tropospheric equatorial zonal wind (m s^{-1}) for the initial wavenumber (left) -1 and (right) -4 perturbation cases in the two-level model under nonlinear heating. The zonal axis is longitude from 0° to 360° ; the vertical axis is the integration time from day 0 to day 30. Solid (dashed) contours are for the westerly (easterly) flows.

tendency for the low-level pressure. As a result, the Kelvin wave propagates eastward.

In the presence of a linear heating, the adiabatic cooling and warming effects have an equal pressure tendency [proportional to $0.1(\partial u/\partial x)$] so that the shape of the Kelvin wave remains unchanged while propagating eastward. This differs significantly from the nonlinear heating scenario in which the effect of the adiabatic warming is 10 times as strong as that of the adiabatic cooling (see Fig. 12, right). As a result, the shape of the initial Kelvin wave is greatly deformed, inducing amplitude and size asymmetries between the low- and high-pressure regions. The deformation of the zonal wind field, on the other hand, is not as strong and fast as that of the pressure field. As a result, an elongated low pressure may overlap with the low-level westerly. Figure 13 shows the zonal structures of the zonal wind

and geopotential height fields at day 0 and day 4. At day 0 the easterly (low pressure) and westerly (high pressure) have the same zonal size and the easterly (westerly) is in phase with the low (high) pressure. Because of the asymmetric effect induced by the nonlinear heating, the zonal length scale of the low pressure becomes greater than that of the high pressure at day 4, while the zonal extent of the easterly is still similar to that of the westerly. This causes a partial overlap between the low pressure and the westerly. The continuous asymmetric forcing eventually leads to the out-of-phase relation between the pressure and zonal wind fields, opposite to the conventional equatorial Kelvin wave phase structure.

How does the frictional boundary layer help keep the in-phase zonal wind-pressure relation? Let us consider the following 2D ($x-z$) governing equations in a 2.5-layer model:

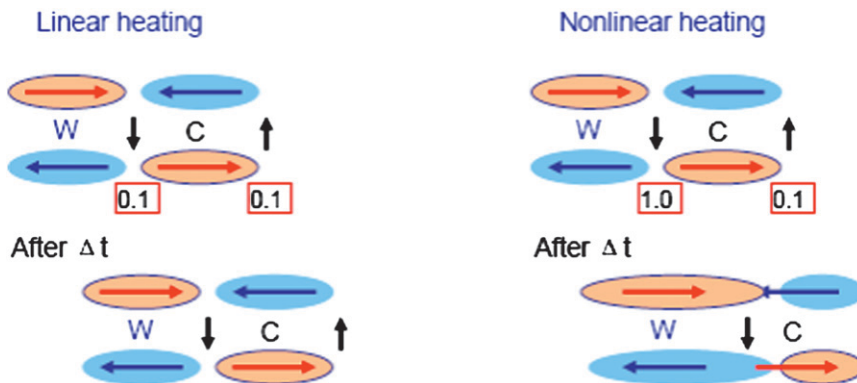


FIG. 12. Schematic diagram for a baroclinic Kelvin wave in the two-level model with (left) linear and (right) nonlinear heating. Blue (red) shadings correspond to low (high) pressure; blue (red) arrows represent easterly (westerly) winds; black arrows represent vertical motion. The value in the red rectangle corresponds to $(1 - \delta I)$, assuming $I = 0.9$.

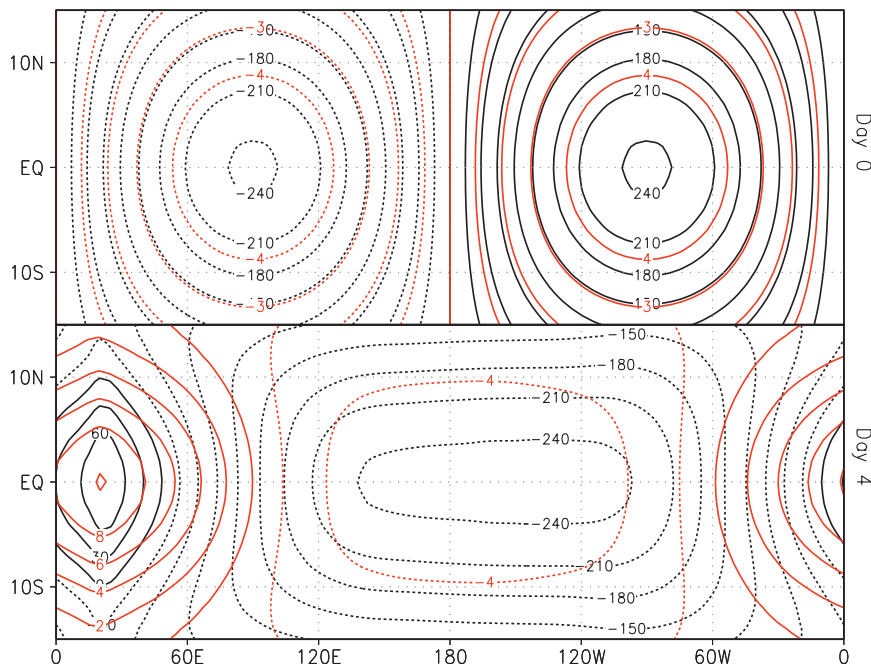


FIG. 13. Horizontal patterns of the lower tropospheric geopotential height (black, m) and zonal wind (red, m s^{-1}) at days (top) 0 and (bottom) 4 for the initial wavenumber-1 case in the two-level model under nonlinear heating. The contour intervals are 30 for the geopotential height and (top) 1 or (bottom) 2 for the zonal wind fields.

$$\frac{\partial u}{\partial t} = -\frac{\partial \phi}{\partial x} \quad \text{and}$$

$$\frac{\partial \phi}{\partial t} + C_0^2(1 - \delta I) \frac{\partial u}{\partial x} = C_0^2(\delta B - 1) \frac{\partial u_B}{\partial x}, \quad \text{where}$$

$$\delta = \begin{cases} 1, & \text{for vertically integrated moisture convergence,} \\ 0, & \text{for vertically integrated moisture divergence.} \end{cases} \quad (4)$$

Here the heating term includes both the lower tropospheric and the boundary layer moisture convergences; u_B is determined by a balance between the zonal pressure gradient and drag. The amplitude of the boundary layer moisture convergence is in general greater than that of the lower tropospheric moisture convergence. Furthermore, there is a zonal phase difference between them. Therefore, the heating associated with the boundary layer frictional convergence is in phase with the lower tropospheric low-pressure center. This makes the heating coefficient δ less asymmetric between the midtropospheric ascending and descending regions and thus reduces the structure asymmetry induced by the nonlinear heating. The zonal wind–pressure in-phase pattern is tightly bounded by the frictional convergence induced heating.

The comparison of the numerical simulations from the two-level and 2.5-layer models confirms the argu-

ment above. Figure 14 shows the zonal wind, geopotential height, and precipitation phase relations from both the models. For the initial wavenumber-1 perturbation case, the zonal wind and pressure fields in both the models are in phase at day 1. Whereas the precipitation center in the two-level model is confined to the zonal convergence zone between the low-level westerly and easterly, the combined effect of the lower tropospheric and boundary layer convergences leads to multiple precipitation centers in the 2.5-layer model. After day 6, the phases of the zonal wind and pressure fields in the two-level model gradually shift; by day 20, the zonal wind and pressure fields are out of phase, completely deforming the Kelvin wave structure. This differs distinctively from the 2.5-layer model, in which the zonal wind and pressure always keep the in-phase relation, with the maximum precipitation peak located over the low-level low-pressure center. The out-of-phase relation between the equatorial zonal wind and pressure leads to westward propagation and no planetary scale selection in the two-level model. Similar phase evolution characteristics appear in the initial wavenumber-4 perturbation case.

One question related to the two-level model simulation is why the deformation of the zonal wind field is not as strong and fast as that of the pressure field. Although the nonlinear heating directly affects the pressure field

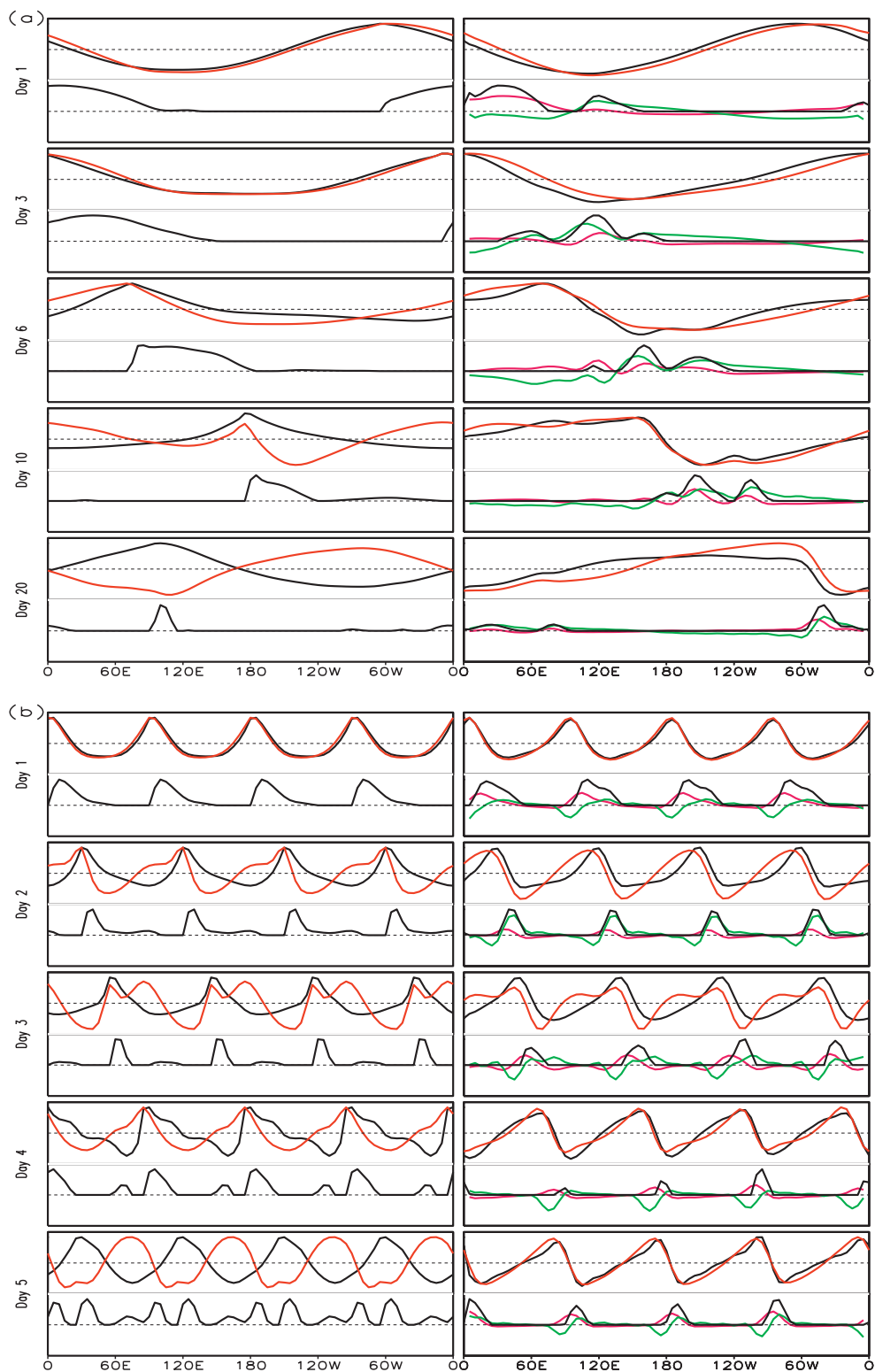


FIG. 14. Equatorial profiles of normalized lower tropospheric zonal wind (red) and geopotential height (upper black line) and precipitation (lower black line), free atmosphere convergence (magenta), and boundary layer frictional convergence (green) for the initial wavenumber (a)-1 and (b)-4 cases from the (left) two-level and (right) 2.5-layer models under nonlinear heating. The dashed line represents the zero line. The zonal mean values of the zonal wind and geopotential height fields have been removed.

(through the thermodynamic equation), it may take some time for winds to adjust to the pressure field. As we know, the quasigeostrophic approximation is valid in the meridional direction even for the equatorial Kelvin waves. According to the geostrophic adjustment theory, if the meridional length scale of a perturbation is much greater than the equatorial Rossby radius of deformation (which is about 1500 km), the wind field may quickly adjust toward the pressure field. In a more realistic scenario in which the length scale is close to or slightly less than the Rossby radius of deformation, the wind adjustment to the pressure field could be slow.

Another question is what causes the westward propagation at the equator. Recall that in a shallow water channel model with two lateral boundaries at $y = 0$ and $y = L$, two types of Kelvin wave solutions may exist. One type of Kelvin wave moves eastward with zonal current and pressure being in phase. Another type of Kelvin wave moves westward while zonal current and pressure are out of phase. At the equator, there are also two types of Kelvin waves in a linear shallow water model. The eastward propagating one has an in-phase zonal wind–pressure relation, whereas the westward propagating one has an out-of-phase relation. In a linear model, only the eastward-propagating equatorial Kelvin wave is physically reasonable because it satisfies a finite meridional boundary condition. The physical explanation of the eastward movement in a two-level first baroclinic model is that because a negative u (easterly) is in phase with a low-pressure center at low-level, the divergence of low-level u leads to descending motion and thus adiabatic warming in the east of the low pressure center, which leads to a negative low-level pressure tendency in situ based on the hydrostatic equation (i.e., the warming leads to an expansion of vertical column and thus to low-level low pressure and/or upper-level high pressure). As a result, the low-level low-pressure center moves eastward. Under the nonlinear heating, the zonal wind and pressure structure deform in such a way that they are out of phase along the equator (i.e., a low-pressure center is collocated with westerly at low levels) while a finite lateral boundary condition is still valid. In this scenario, the low-level westerly would lead to a descending motion and adiabatic warming to the west of the low-level low pressure center, thus causing the westward propagation.

The numerical results above indicate that both the nonlinear heating and the frictional boundary layer are essential for the MJO planetary scale selection. The frictional boundary layer in general has the following two effects: First, it is crucial for the destabilization of the MJO. Second, it helps reduce the structure asym-

metry caused by the nonlinear heating and retain the pressure–zonal wind in-phase relationship.

5. Sensitivity experiments

In this section we examine the sensitivity of the 2.5-layer model solution to the background surface specific humidity, the model horizontal resolution, and the free atmospheric damping coefficient.

Two sensitivity experiments are performed with different mean surface specific humidity values, 14 and 16 g kg^{-1} , compared to 18 g kg^{-1} in the control experiment. The change of the mean specific humidity does not alter the characteristic of the planetary scale selection, even though the propagation speed and the growth rate change. The larger the humidity is, the slower the wave propagates and the faster the perturbation grows (Fig. 15).

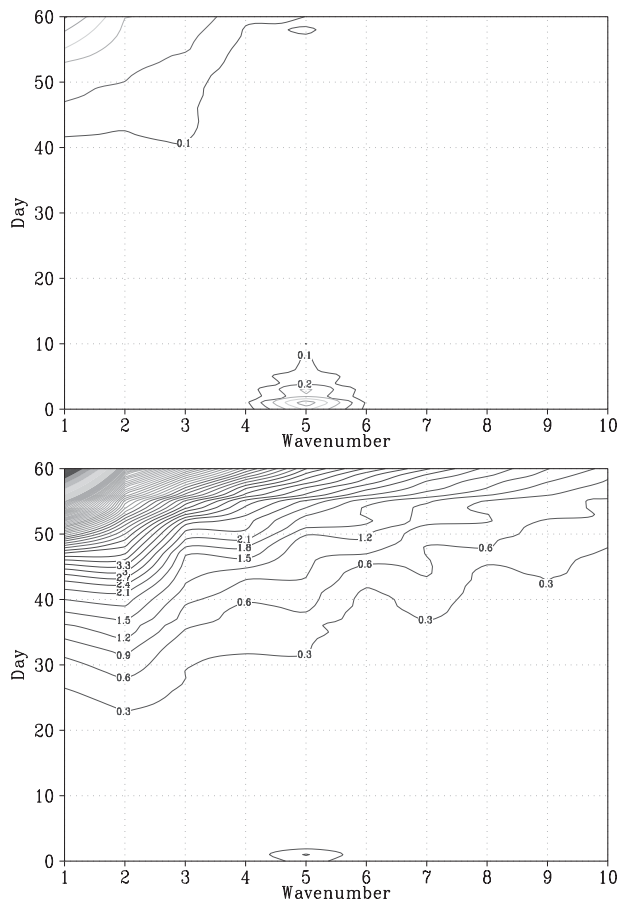


FIG. 15. Time evolution of wavenumber-1–10 Fourier coefficients of the lower tropospheric zonal wind in the 2.5-layer model under nonlinear heating with specified mean specific humidity values of (top) 14 and (bottom) 16 g kg^{-1} . The contour interval is (top) 0.1 and (bottom) 0.3 m s^{-1} . An initial wavenumber-5 perturbation is specified.

This is physically understood because the growth rate increases with enhanced moisture convergence and the phase propagation speed is reversely proportional to the surface moist static energy (Li and Wang 1994a,b).

The horizontal resolution ($5^\circ \times 2^\circ$) in the control experiments is relatively coarse. To examine whether the coarse resolution may partially contribute to the planetary scale selection, we conduct the second set of sensitivity experiments. Because our focus is on the scale selection in the zonal direction, the zonal resolution is of the main concern. We keep the same meridional resolution but increase the zonal resolution from 5° to 2° and 1° , respectively. The numerical results show that the preferred planetary zonal scale is well reproduced in all the sensitivity experiments, suggesting that the scale selection process elaborated here is not resolution dependent, even though the growth rate increases slightly with the increased model resolution.

A key variable in the scale selection process is the free atmospheric Newtonian damping or Rayleigh friction coefficient. To test the model solution to the damping coefficient, we conducted an additional sensitivity experiment when initially a wavenumber-3 perturbation is specified. All the parameters are same as those in the control experiment except that the free atmosphere friction or damping coefficient is increased by one order of magnitude. The reason for this big increase in the

damping coefficient is to reveal a clearer difference. (Note that because the model contains various forms of damping such as horizontal diffusion and smoothing, a smaller increase in the Rayleigh friction or Newtonian damping does not greatly affect the model's total dissipation.) Figure 16 shows the time–longitude section of the simulated low-level zonal wind at the equator for both the control and sensitivity experiments. At day 25, a wavenumber-1 structure appears in the control experiment, whereas there is still a dominant wavenumber-3 structure in the sensitivity experiment. A further diagnosis of the model output reveals that the horizontal extent of the Kelvin–Rossby wave couplet is indeed greatly reduced in the presence of the strong damping, which allows shorter wavelength perturbations to survive. Thus, the sensitivity numerical experiment confirms the aforementioned scale selection mechanism.

6. Summary

A 2.5-layer model and a two-level model are employed to study the role of the nonlinear, positive-only heating and the frictional boundary layer in the planetary scale selection of MJO. Our strategy is to specify an initial perturbation that has the form of an equatorial Kelvin wave at zonal wavenumbers 1, 2, ..., 15, respectively and to examine how the perturbation evolves

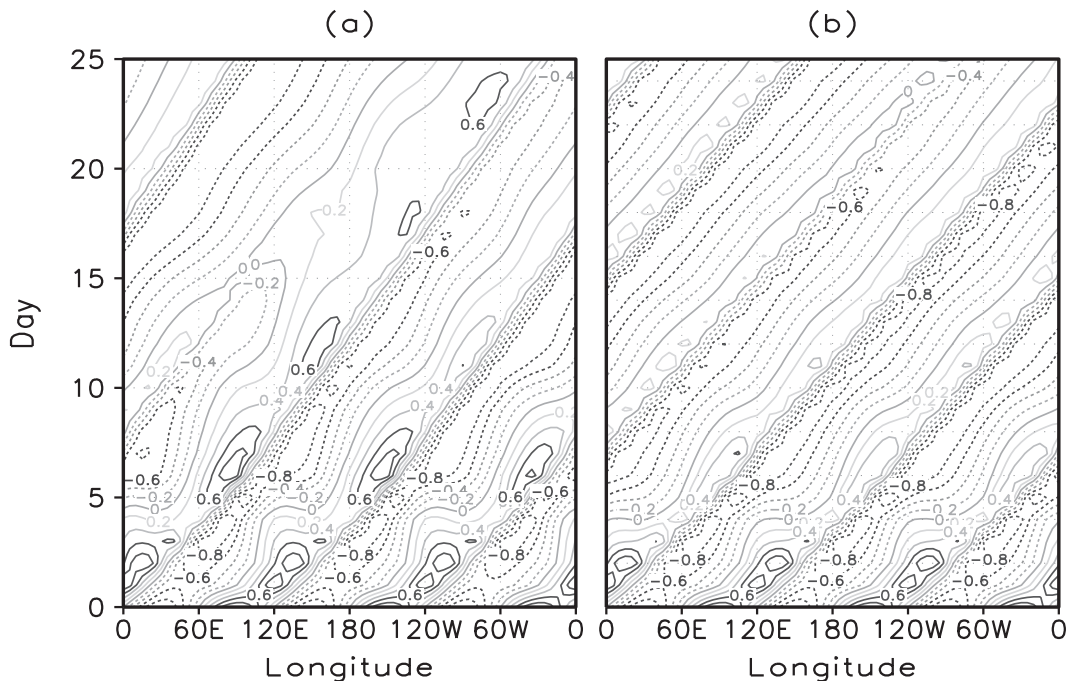


FIG. 16. Time–longitude cross section of the normalized low-level zonal wind along the equator in the 2.5-layer model under nonlinear heating for (a) the control experiment and (b) a sensitivity experiment in which the free atmospheric Rayleigh friction or Newtonian damping coefficient is increased to $2 \times 10^{-5} \text{ s}^{-1}$.

with time in the presence of linear or a nonlinear heating. The convective heating in both the models is proportional to the vertically integrated moisture convergence.

The numerical simulations show that the perturbation behaves differently for linear and nonlinear heating in the 2.5-layer model. Whereas the linear heating prefers the most unstable mode at shorter wavelength, the nonlinear heating leads to the planetary zonal scale selection in the model.

The mechanism for the planetary scale selection under the nonlinear heating is summarized as follows: The positive-only conditional heating leads to distinctive phase speeds between the dry Kelvin wave and the moist Kelvin–Rossby wave couplet. The fast dry Kelvin wave excited by a convective branch may catch up and suppress another convective branch (which travels at a slower phase speed of the wet Kelvin–Rossby wave couplet) ahead of it, as long as the zonal distance between the two convective branches (i.e., the wavelength of the perturbation) is smaller than a critical distance (Gill 1982). It is the interference between the dry Kelvin wave and the wet Kelvin–Rossby wave couplet that causes the dissipation of shorter wavelength perturbations and leads to the longwave selection. The effect of the nonlinear heating discussed above resembles to a certain degree the behavior of Burger's equation in the sense that the phase speed depends on the sign of the perturbation, which tends to produce the similar behavior seen in Fig. 9.

A comparison of simulations from the 2.5-layer model and a two-level model reveals that the frictional boundary layer is another crucial factor for the planetary scale selection. Without the PBL, there is no planetary scale selection even in the presence of the nonlinear heating. This is because the positive-only heating in the two-level model causes a structure asymmetry between the wet and dry regions, which eventually leads to an out-of-phase relation between the zonal wind and pressure fields at the equator. The out-of-phase zonal wind–pressure pattern causes the westward propagation of the equatorial perturbation while the amplitude of the perturbation decays.

Therefore, a necessary and sufficient condition for the MJO planetary scale selection is the presence of both nonlinear heating and a frictional boundary layer. Lacking either would lead to no planetary scale selection. This implies that a minimum model that describes the essential dynamics of MJO is the first-baroclinic-mode free atmosphere interacting with a well-mixed boundary layer. Whereas the positive-only heating is essential for shortwave cutoff by differentiating dry and wet Kelvin wave speeds, the boundary layer plays a primary role in 1) destabilizing the MJO through the frictional moisture convergence and 2) keeping the equatorial zonal wind–

pressure in-phase structure through the modulation of the phase of convective heating.

The sensitivity experiments with different background moisture and model resolution indicate that the planetary scale selection for MJO is not sensitive to the change of the parameters. Because the simple models do not consider the radiation–convection feedback, the stationary oscillatory mode is not reproduced. The period of the traveling MJO mode may be determined by its zonal wavelength and phase propagation speed and is about 30–50 days under a realistic model parameter regime.

It is worth mentioning that the current convection scheme in the model is very crude; the vertically integrated moisture convergence is likely a response and feedback to diabatic heating rather than a root cause. It will be interesting to see how sensitive the model solution is to the different convective schemes. The interaction between the first and second baroclinic modes through convective momentum transport in the Majda and Stechmann (2009) model is to a large extent similar to the interaction between the PBL and free atmosphere in the current model. The major difference between the two frameworks lies in that the former emphasizes the effect of upscale and downscale nonlinear momentum transport in a nonrotational fluid, whereas the latter stresses the importance of the nonlinear heating in an equatorial beta plane where Rossby waves are crucial in coupling with Kelvin waves in maintaining the diabatic heating. Another relevant work is the moisture-stratiform instability of the equatorially trapped convectively coupled waves (Kuang 2008; Andersen and Kuang 2008). The effect of the 3D mean flow on the MJO scale selection is not considered in the current model. As we know, at the equator the mean flow exhibits a Walker-type wavenumber-2 structure, with rising branches over the western Pacific and Atlantic warm pools. How such a mean flow modulates the MJO longwave scale selection would be another interesting dynamic question.

Acknowledgments. This research was supported by the NSFC Grants 40628006/40675055 and ONR Grants N000140710145/N000140810256 and by the International Pacific Research Center, which is sponsored by the Japan Agency for Marine–Earth Science and Technology (JAMSTEC), NASA (NNX07AG53G), and NOAA (NA17RJ1230).

REFERENCES

- Andersen, J. A., and Z. Kuang, 2008: A toy model of the instability in the equatorially trapped convectively coupled waves on the equatorial beta plane. *J. Atmos. Sci.*, **65**, 3736–3757.

- Biello, J. A., and A. J. Majda, 2005: A new multiscale model for the Madden-Julian Oscillation. *J. Atmos. Sci.*, **62**, 1694–1721.
- , —, and M. W. Moncrieff, 2007: Meridional momentum flux and superrotation in the multiscale IPESD MJO model. *J. Atmos. Sci.*, **64**, 1636–1651.
- Chang, C.-P., 1977: Viscous internal gravity waves and low-frequency oscillations in the tropics. *J. Atmos. Sci.*, **34**, 901–910.
- , and H. Lim, 1988: Kelvin wave-CISK: A possible mechanism for the 30–50-day oscillations. *J. Atmos. Sci.*, **45**, 1709–1720.
- Gill, A. E., 1980: Some simple solutions for heat-induced tropical circulation. *Quart. J. Roy. Meteor. Soc.*, **106**, 447–462.
- , 1982: *Atmosphere–Ocean Dynamics*. Academic Press, 666 pp.
- Goswami, P., and R. K. Rao, 1994: A dynamical mechanism for selective excitation of the Kelvin mode at time scales of 30–50 days. *J. Atmos. Sci.*, **51**, 2769–2779.
- Grabowski, W. W., 2001: Coupling cloud processes with the large-scale dynamics using the cloud-resolving convection parameterization (CRCP). *J. Atmos. Sci.*, **58**, 978–997.
- Hendon, H. H., and M. L. Salby, 1994: The life cycle of the Madden-Julian oscillation. *J. Atmos. Sci.*, **51**, 2225–2237.
- Khouider, B., and A. J. Majda, 2006: A simple multicloud parameterization for convectively coupled tropical waves. Part I: Linear analysis. *J. Atmos. Sci.*, **63**, 1308–1323.
- , and —, 2007: A simple multicloud parameterization for convectively coupled tropical waves. Part II: Nonlinear simulations. *J. Atmos. Sci.*, **64**, 381–400.
- Kuang, Z., 2008: A moisture-stratiform instability for convectively coupled waves. *J. Atmos. Sci.*, **65**, 834–854.
- Lau, K.-M., and L. Peng, 1987: Origin of low-frequency (intra-seasonal) oscillations in the tropical atmosphere. Part I: Basic theory. *J. Atmos. Sci.*, **44**, 950–972.
- Li, T., and B. Wang, 1994a: The influence of sea surface temperature on the tropical intraseasonal oscillation: A numerical study. *Mon. Wea. Rev.*, **122**, 2349–2362.
- , and —, 1994b: A thermodynamic equilibrium climate model for monthly mean surface winds and precipitation over the tropical Pacific. *J. Atmos. Sci.*, **51**, 1372–1385.
- Lim, H., T.-K. Lim, and C.-P. Chang, 1990: Reexamination of wave-CISK theory: Existence and properties of nonlinear wave-CISK modes. *J. Atmos. Sci.*, **47**, 3078–3091.
- Madden, R. A., and P. R. Julian, 1971: Detection of a 40–50-day oscillation in the zonal wind in the tropical Pacific. *J. Atmos. Sci.*, **28**, 702–708.
- , and —, 1972: Description of global-scale circulation cells in the tropics with a 40–50 day period. *J. Atmos. Sci.*, **29**, 1109–1123.
- Majda, A. J., and J. A. Biello, 2004: A multiscale model for tropical intraseasonal oscillations. *Proc. Natl. Acad. Sci. USA*, **101**, 4736–4741.
- , and S. N. Stechmann, 2009: A simple dynamical model with features of convective momentum transport. *J. Atmos. Sci.*, **66**, 373–392.
- Maloney, E. D., 2002: An intraseasonal oscillation composite life cycle in the NCAR CCM3.6 with modified convection. *J. Climate*, **15**, 964–982.
- Matsuno, T., 1966: Quasigeostrophic motions in the equatorial area. *J. Meteor. Soc. Japan*, **44**, 25–43.
- Moncrieff, M., 2004: Analytic representation of the large-scale organization of tropical convection. *J. Atmos. Sci.*, **61**, 1521–1538.
- Nakazawa, T., 1988: Tropical super clusters within intraseasonal variations over the western Pacific. *J. Meteor. Soc. Japan*, **66**, 823–839.
- Waliser, D. E., K. M. Lau, and J.-H. Kim, 1999: The influence of coupled sea surface temperatures on the Madden-Julian oscillation: A model perturbation experiment. *J. Atmos. Sci.*, **56**, 333–358.
- Wang, B., 1988: Dynamics of tropical low-frequency waves: An analysis of moist Kelvin waves. *J. Atmos. Sci.*, **45**, 2051–2065.
- , and Y. Xue, 1992: Behavior of a moist Kelvin wave packet with nonlinear heating. *J. Atmos. Sci.*, **49**, 549–559.
- , and T. Li, 1993: A simple tropical atmosphere model of relevance to short-term climate variations. *J. Atmos. Sci.*, **50**, 260–284.
- , and —, 1994: Convective interaction with boundary-layer dynamics in the development of a tropical intraseasonal system. *J. Atmos. Sci.*, **51**, 1386–1400.
- , and X. Xie, 1997: A model for boreal summer intraseasonal oscillation. *J. Atmos. Sci.*, **54**, 72–86.
- Xie, S.-P., 1994: On preferred zonal scale of wave-CISK with conditional heating. *J. Meteor. Soc. Japan*, **72**, 19–30.